In plane behaviour of rammed earth under cyclic loading: experimental testing and finite element modelling

Lorenzo Miccoli [a,*], Anastasios Drougkas [b], Urs Müller [c]

[a] Bundesanstalt für Materialforschung und –prüfung (BAM), Division Building Materials, Unter den Eichen 87, 12205 Berlin, Germany.

[b] Department of Structural Engineering, National Technical University of Athens, Laboratory of Reinforced Concrete, 5, Iroon Polytechniou Str., 15773 Zografou, Greece.

[c] CBI Swedish Cement and Concrete Research Institute, c/o SP, Box 857, Brinellgatan 4, 50462 Borås, Sweden.

*Corresponding author. Tel. +49 30 8104 3371; Fax +49 30 8104 1717; E-mail address: lorenzo.miccoli@bam.de

Abstract

The intent of this paper is to numerically simulate the in-plane behaviour of rammed earth walls under cyclic shear-compression tests. The experimental testing allowed obtaining the maximum horizontal loads, the displacement capacity and the level of non-linear behaviour of the respective load-displacement relationships as well as the failure modes. The calibration of the numerical model (finite elements method) was carried out using the experimental results. A micro modelling approach was considered. The behaviour of rammed earth material was simulated using a total strain rotating crack model. A Mohr-Coulomb failure criterion was used to reproduce the behaviour of the interfaces between layers.

Although the results of the numerical model well fit the experimental results a sensitivity analysis was performed to define also the influence of different input parameters. As expected the sensitivity analysis shows that the occurrence of sliding failure is mainly influenced by two parameters of the interface elements: the tensile strength and the friction angle. Moreover the cohesion and the layers thickness show a limited influence on the shear behaviour.

Keywords: rammed earth, in-plane loads, shear behaviour, cyclic shear-compression tests, finite element modelling, pseudo-dynamic tests

NOTATION

c	cohesion coefficient (N/mm^2)
E	Young's modulus (N/mm^2)
f_c	uniaxial compressive strength (N/mm^2)
f_t	tensile strength (N/mm^2)
f'_t	interface tensile strength (N/mm)
G	shear modulus (N/mm^2)
G_c	compressive fracture energy (N/mm)
G^I_f	tensile fracture energy (N/mm)
$G^I_{f,crack}$	interface tensile fracture energy (N/mm)
H	horizontal load (kN)
H_{cr}	horizontal load at crack limit state (kN)
H_f	horizontal load at flexural cracking limit (kN)
H_{max}	maximum horizontal load (kN)
H_u	horizontal load at ultimate displacement (kN)
k_n	interface normal stiffness (N/mm^3)
k_s	interface tangential stiffness (N/mm^3)
RH	relative humidity (%)
t	time (sec)
V	vertical load (kN)
δ	displacement (mm)
δ_{cr}	displacement at crack limit state (mm)
δ_f	displacement at flexural cracking limit (mm)
δ_{max}	displacement at maximum horizontal load (mm)
δ_u	ultimate displacement (mm)
σ	vertical stress (N/mm^2)
σ_{max}	mean compressive strength (N/mm^2)
τ	shear stress (N/mm^2)

τ_{max}	nominal shear strength (N/mm^2)
θ_{cr}	rotation angle at crack limit state (%)
θ_f	rotation angle at flexural cracking limit (%)
θ_{Hmax}	rotation angle at maximum horizontal load (%)
θ_u	rotation angle at ultimate displacement (%)
ν	Poisson's ratio (-)
φ	internal friction angle (°)
ψ	dilatancy angle (°)

1. INTRODUCTION

Earthen buildings represent an important part of cultural heritage. Earthen materials are among the oldest materials used in construction, and perhaps the least understood in terms of its strength and deformation properties. This statement is indeed true since the role of role earthen materials as a structural or non-structural material is often obscured.

The intent of this paper is to investigate the mechanical behaviour of rammed earth walls under in-plane cyclic shear-compression tests. The goal of the experiments was to test the general response of monolithic rammed earth walls under pseudo-dynamic horizontal loading in terms of lateral load increase and displacement capacity. Rammed earth is an earthen construction technique in which moistened earth is compacted in consecutive layers within a wooden formwork.

The compaction process provides to the rammed earth a distinctive layered structure. Often the single formwork lifts can be recognised. In cases where the clay content of the earth is too low or the grain size distribution is not optimal lime was often added to the rammed earth mix or filled into the formwork in layers [1].

The layered structure influences the crack mechanics but the mechanical behaviour of rammed earth seems not to be distinctively anisotropic [2]. Although some numerical models for earthen structures can be developed, their correlation to real-life situations or experiments as a means of verification and validation has yet to be thoroughly analysed.

However only few testing campaigns on pseudo-dynamic horizontal loading, aiming at defining quantitative properties, were carried out to better understand the behaviour of rammed earth under cyclic load.

Walker and Morris [3] tested rammed earth walls stabilised with 10% cement and reinforced with steel rods under in-plane cyclic loading. Hamilton [4] performed tests on 3% cement stabilised rammed earth walls with and without post tensioned strengthening both in plane and out of plane. These walls were built with concrete caps and bases.

These campaigns carried out offered limited data to develop reliable non-linear models. Moreover most of the few studies on modelling rammed earth with finite element modelling (FEM) were used to predict stress levels and to simulate possible collapse mechanisms [2][5][6]. So far only one study on the numerical modelling of rammed earth walls subjected to in-plane horizontal loading is available [7]. This study reproduces the brittle characteristics of rammed earth using deformable plane elements and linkage elements.

In the first part of the paper the characterisation of the mechanical behaviour of rammed earth walls tested under in-plane cyclic shear-compression loads is presented. The mechanical properties obtained were used as the basis for FEM.

The numerical modelling of the rammed earth walls tested is presented in the second part. A non-linear constitutive law based on the total strain rotating crack model (TSRCM) was employed as implemented in the DIANA software package [8]. This model was used successfully in a previous study to simulate the rammed earth behaviour under uniaxial and diagonal compression [9], and is relatively common in nonlinear FEM analysis of several brittle materials, such as concrete or masonry. The aim of the numerical analysis is to simulate the behaviour of rammed earth under in-plane horizontal cyclic loading. The micro-modelling approach was considered for the simulation of the experimental tests, and the respective FEM model was calibrated according to the experimental results. This approach allowed assessing the influence of the apparent weakness of the interfaces between layers on the shear behaviour of rammed earth.

The goal of the numerical simulation of the tests is the determination of the adequacy of established methods used in masonry analysis for the analysis of rammed earth, a material that shares the brittle characteristics of masonry materials and is used in geometrical typologies, such as walls, common in masonry construction. In addition to the simulation of the present experimental tests, a parametric analysis is performed with the purpose of determining the sensitivity of the response of rammed earth walls to changes in numerous material parameters.

2. EXPERIMENTAL PROGRAMME

2.1 Materials and preparation of the samples

Three rammed earth walls were manufactured at BAM and used for cyclic shear-compression tests. A local manufacturer of prefabricated earthen materials (Claytec GmBH, Germany) provided the earth used for the samples. The rammed earth walls of size 1300 mm × 1050 mm × 250 mm show a bulk density of 2,190 kg/m^3, a particle size range of 0–16 mm and shrinkage of 0.5% During the manufacturing process fairly dry earth (moisture content 9–10%) was mechanically compacted in thirteen layers within a plywood formwork using a mechanical rammer. At the end of the compaction the walls shows an average layer thickness of about 100 mm.

After production, the walls were stored for two months in the laboratory for drying. Before testing the walls showed a final equilibrium moisture content in the range of 2–3%.

Mechanical properties of rammed earth under static tests were determined in the BAM laboratories on wallettes (500 mm × 500 mm × 100 mm) and on cubes (100 mm × 100 mm × 100 mm). The wallettes' results showed a uniaxial compressive strength σ_{max} of 3.73 N/mm^2 and a shear strength τ_{max} of 0.70 N/mm^2. The Young's modulus E and the shear modulus G, determined as a secant-modulus of the stress at 1/3 of the maximum load, were respectively of 4143 N/mm^2 and 1582 N/mm^2. Cubes' results showed a uniaxial compressive strength f_c of 3.32 N/mm^2. The detailed descriptions of the materials characterisation and static tests are reported elsewhere [10].

2.2 Test setup

Three cyclic in-plane shear-compression tests were carried out at the Institute of Theoretical and Applied Mechanics (ITAM) in Prague. The samples were placed into a testing rig able to provide simultaneously uniform compression and cyclic horizontal loads at the top of the sample. The base of the walls was fixed and the top end was free to rotate. The test setup shows the position of the linear variable differential transformers (LDVTs) used to measure displacements (Fig. 1).

A vertical compression load V of 140 kN, representing a σ of 0.56 N/mm^2, was transferred to the wall through three hydraulic jacks by a steel capping beam at the top of the sample. This vertical load level was chosen to obtain the shear type behaviour. An actuator at the top of the wall provided a horizontal cyclic load

with a defined displacement on the sample at a frequency of 0.1 Hz in sequences of three cycles. During horizontal loading cycles the vertical load was kept constant.

After every sequence the displacement was increased by 2.5 mm to a maximum of 12.5 mm.

The displacements at the bottom (P6) and top (P5) of the wall and the diagonal deformations (P1–P4) on both sides were measured. Loading was ended when, at the controlled deformation, the horizontal load started to decrease.

2.3 Test results

The walls' behaviour was idealised using the performance-based engineering criteria proposed by Abrams [11]. The tests campaign showed four limit states, representing the change of the wall behaviour under the progressive increase of applied horizontal displacement. The cracks, localised in the two diagonal lines of the walls, show the typical X-shaped crack pattern (Fig. 1).

A typical hysteresis loop of the horizontal load and the corresponding displacement obtained from the cyclic curves for each step of loading is reported in Fig. 3. The graph shows both the tension and the compression part of the cyclic curves.

In the shear-compression envelope curves (Fig. 4) only the compression part of envelope curve is reported, in this case the horizontal load is higher than for the tension part. However similar results could be obtained also for the tension part. All measured load-displacement envelopes show a shape typical of shear failure due to the limited sliding mechanism of rammed earth layers. The test results show a H_{max} in the range of 60–78 kN and a δ_{max} in the range of 6.1–7.1 mm.

Table 1 lists the values of lateral loads (H) and corresponding rotation angles (θ) at the four limit states, the main load and observed failure modes. The graph shows the maximum lateral load values and the corresponding maximum displacement values obtained from the walls. The first non-linearity, due to the first flexural cracks opening at the bottom bed joints (flexural cracking limit, H_f, δ_f), occurred at displacements of about 1.6–1.8 mm (mean rotation angle θ_f = 0.13%). The second non-linearity took place at the following crack limit state (H_{cr}, δ_{cr}) when the first diagonal crack opened. This state occurred at displacements of about 3.2–3.9 mm (mean rotation angle θ_{cr} = 0.30%).

Subsequently loads increased gradually until maximum load (H_{max}) and the relevant displacement (δ_{max}) were reached. This condition represents the third limit state, and is characterised by the formation of a diagonal strut, defined by cracks which crossed rammed earth layers.

3. NUMERICAL MODELLING

3.1 Initial considerations (geometry, boundary conditions and loading)

Numerical analyses for the simulation of the experimental tests were carried out using nonlinear FEM. The micro-modelling approach was adopted for the creation of the model. According to this approach the rammed earth layers were modelled using continuum elements and the interaction between the layers themselves and with the bounding structures at the base and the top of the wall were modelled using interface elements. Following these assumptions the rammed earth as a whole is taken as an anisotropic material, rather than as isotropic [12], the anisotropy resulting from the inclusion of horizontal interfaces. The continuum was modelled using 8-node quadrilateral plane stress elements, plane stress being a reasonable and computationally cost-effective assumption for the given geometrical arrangement, loading and materials, and the discontinuum parts were modelled using 6-node line interface elements. The DIANA finite element package was used for the preparation of the model and the execution of the analyses [8].

In addition to the layers, two stiff bounding beams were considered in the model: one serving as a foundation and one as a top restraint. The base beam was fixed at its foundation and connected to the lowermost rammed earth layer via an interface. The top bounding beam was similarly connected to the uppermost rammed earth layer, but was left free to translate and rotate, as per the experimental conditions. Overall, 1323 plane stress and 378 interface elements were used in the finite element mesh. The vertical load was applied uniformly distributed at the top of the bounding beam. The cyclic horizontal load was applied as a displacement of the top bounding beam at the top of the wall.

3.2 Constitutive laws

A TSRCM was assigned to the continuum elements. This model is able to model the nonlinear behaviour of the rammed earth layers in tension and compression. For the former a multi-linear curve matching the experimental curves obtained for the materials was assumed [13] and for the latter an exponential softening curve, both based on fracture energy and finite element crack bandwidth. The tensile failure criterion is

evaluated in the direction of the maximum principal strain and the direction of the crack is fixed upon formation, which is a rational assumption for brittle materials, such as rammed earth layers. Secant unloading and reloading is assumed. Linear elasticity is assumed for the base and top beam.

A Mohr-Coulomb frictional failure criterion with a tension cut-off was assigned to the interface elements. This criterion allows the simulation of the behaviour of the interfaces in combined tension and shear. These interfaces do not represent a physical structural entity, such as a mortar joint, but model the interaction of the rammed earth layers with each other and with the base and top beam.

3.3 Calibration of the model and results

To the rammed earth layers were assigned material properties as determined experimentally and fitted through calibration to existing data [13]. Since no mechanical characterisation of the layers interfaces was carried out, nominal values were used for the frictional and tension properties of the interfaces. The elastic properties of the interfaces, namely their elastic stiffness in tension and shear, were determined through calibration and matching of the numerical to the experimental results. Ideally, the interfaces ought to be rigid until sliding or opening between the layers occurs. This requires prescribing a high dummy stiffness to the interface. However, due to imperfections in the compaction, imperfect contact between layers and disturbance of the interface in the actual structure, this assumption results in a numerical overestimation of the global stiffness. The normal stiffness of the interfaces had to therefore be reduced. The shear stiffness is derived from the normal stiffness according to the equation (1):

$$k_s = \frac{k_n}{2(1+\nu)} \tag{1}$$

where ν is the Poisson's ratio of the rammed earth layer material. All the material properties used in the initial analysis are summarised in Table 2.

The results obtained from the numerical analysis are presented in Fig. 5. The peak shear force is predicted with good accuracy, although the global stiffness of the structure is overestimated in the initial cycles. The agreement between the experimental and the numerical curves is better in the subsequent cycles.

The crack pattern obtained at the end of the last loading sequence is given in Fig. 6, where the orientation of the cracks and the visualisation of the relative crack sizes are shown. The failure mode is dominated by distinct diagonal cracking, in good agreement with the experimentally obtained failure of the layers. Some damage at the interfaces was also registered at the early stages of the analysis. The cracking damage at the

end of the 2.5 mm sequence was negligible. After the marked opening of the diagonal crack at the top right of the wall at the end of the 7.5 mm sequence, its width increases at the end of each subsequent sequence.

The micro-model allowed capturing the failure by delamination of the interfaces between layers, similar to the one observed in the experimental tests. This revealed to be the main advantage of the micro-model approach, the model being sufficiently accurate to simulate the global cyclic behaviour of the rammed earth walls tested. This approach requires the definition of adequate stress-strain relationships. The use of the micro-modelling approach, where an additional computational effort is required, is justified when specific collapse mechanisms involving failure of the interfaces between layers are expected. In comparison with the previous numerical study [9] the interface stiffness here adopted presents significant differences. The interfaces need to be prescribed a lower elastic stiffness than the interfaces used to reproduce the shear behaviour under diagonal compression.

4. SENSITIVITY ANALYSIS

Based on the initial numerical results, a parametric investigation was carried out, focused on the influence of several material properties on the response of the structure to the prescribed cyclic loading. This analysis was motivated by a variety of reasons. First, a relatively high degree of variability in the mechanical property characterisation of the layers and the interfaces is expected, due to the nature of the production of these materials. Second, certain mechanical tests, such as those for the characterisation of the interfaces, were not carried out. Lastly, the wide range of parameter variability employed serves in providing indicative results for walls composed of rammed earth with potentially different properties. The sensitivity analysis was carried out considering the parameters variation listed in Table 3.

A previous parametric investigation carried out along the same lines on the shear strength under diagonal compression of rammed earth samples revealed sensitivity to the compressive strength, the Poisson's ratio, the tensile strength and the tensile fracture energy of the layers and to the cohesion of the interfaces. In the present study the numerical results exhibited sensitivity to the properties of the layers, but the influence of the cohesion in the interfaces was not so pronounced.

The influence of the parameters variation on the horizontal load capacity is given in Fig. 7. A decrease in the tensile fracture energy resulted in a dramatic decrease of the response, particularly in the higher width cycles, while it resulted in a maintaining a high reaction force at those same cycles when increased. The increase of

tensile strength had a similar effect, but its decrease led to the premature cracking of the layers and a decrease in the response of the early contraction cycles. A Poisson's ratio ν decrease led to an increase in the reaction force for the wider cycles, while a ν increase led to the opposite result. Finally, the compressive strength of the layers had a more limited effect, and in fact a decrease of this value led to an increase in the reaction force for some of the retraction cycles.

Concerning the properties of the layers, the above results indicate that the response of the wall is dominated by tensile cracking rather than crushing in compression. A higher tensile strength and fracture energy resulted in a very similar compression and retraction envelope.

The synthetic results of the sensitivity analysis are summarised in Table 3 concerning the effects on the horizontal load capacity of the rammed earth wall.

The sensitivity analysis performed showed that the tensile fracture energy and tensile strength are the parameters with the greatest influence on the maximum shear stress of the wall. Thus, experimental investigations of the mechanical behaviour of rammed earth should address carefully the determination of the aforementioned parameters. The strong influence of these material parameters indicate a sensitivity of the global response to effects related to cracking in tension. Regarding the parameters of the interface elements, the tensile strength and the friction angle are shown as critical parameters in relation to the sliding failure. On the other hand, the cohesion showed a little influence on the shear behaviour.

5. CONCLUSIONS

The experimental characterisation and numerical simulation of rammed earth walls under cyclic loading are here presented. In the first part the non-linear behaviour of rammed earth was assessed through an experimental programme based on pseudo-dynamic testing. In the second part the micro-modelling approach was used to model the non-linear behaviour of rammed earth. Based on the positive results on modelling rammed earth shear behaviour under diagonal compression test in a previous study [9] the TSRCM was used to simulate the behaviour of the rammed earth material, while the Mohr-Coulomb failure criterion was used to model the interfaces between layers. The first results showed that the calibrated numerical model fitted the experimental hysteresis loops and their damage pattern well. Although numerical results calibrated with the

experimental results were satisfactory, a sensitivity analysis was performed to assess the influence of different input parameters on the global shear behaviour.

A better understanding of the modelling of rammed earth walls with the TSRCM and the Coulomb friction model was provided thanks to the model calibration and the sensitivity analysis performed. In particular these two phases were preparatory for the definition of the stress-strain relationships and their respective parameters.

The numerical simulation of rammed earth requires the definition of the multi-linear relationship (f_c and E) and the Poisson's ratio ν through a complete characterisation of the compression behaviour. Additional testing is required to define the parameters in tension and of the interfaces between layers. In some cases the complexity to obtain all these parameters in the experimental phase suggest to provide a list of recommended values for the parameters in the model (Table 4). These parameters were obtained using the results of the compression tests carried out in a previous study [9], integrated with the results of the cyclic shear-compression tests and the numerical analysis performed in this paper. Although this table represents a good base to perform a reliable FEM of rammed earth walls, more experimental data should be collected to refine the recommended values and for proposing other relations between parameters. In conclusion the numerical modelling of full-scale walls subjected to shaking table tests could represent an important development for the validation of the modelling approach here proposed.

ACKNOWLEDGEMENTS

This research was funded by the European Commission within the framework of the project NIKER dealing with improving immovable Cultural Heritage assets against the risk of earthquakes (contract No. 244123). The authors wish to express their gratitude to Mr. André Gardei, Dr. Stanislav Pospíšil and Mr. Shota Urushadze for their important support in the test setup.

REFERENCES

[1] Ciancio D, Beckett CTS, Carraro JAH (2014) Optimum lime content identification for lime-stabilised rammed earth. Constr Build Mater 53:59–65

[2] Jaquin PA, Augarde CE, Gerrard CM (2006) Analysis of historical rammed earth construction. In: Proceeding of 9th young geotechnical engineers conference 2006, Belfast

[3] Walker R, Morris H (1998) Development of new performance based standards for earth building. In: Proceedings of the Australasian Structural Engineering Conference, Auckland, pp 477–484

[4] Hamilton III HR, McBride J, Grill J (2006) Cyclic testing of rammed-earth walls containing post-tensioned reinforcement. Earthquake Spectra 22:937–959

[5] Gomes I, Lopes M, Brito J (2012) Seismic resistance of earth construction in Portugal. Eng Struct 33:932–941

[6] Jaquin PA, Augarde CE, Gerrard CM (2004) Analysis of Tapial structures for modern use and conservation. In: Proceedings of 4th international conference on structural analysis of historical constructions, 10–13 November, Padova, Italy, pp 1315–1321

[7] Zangmo D, Tsubaki T (2008) Failure behavior of reinforced rammed earth walls subjected to in-plane horizontal loading. In: Proceedings of JCI 30:1651–1656

[8] TNO (2009) Displacement method analyser (DIANA) user's manual. Release 9.4, Netherlands

[9] Miccoli L, Oliveira DV, Silva RA, Müller U, Schueremans L (2015) Static behaviour of rammed earth: experimental testing and finite element modelling. Mater Struct: 48, 3443–3456.

[10] Miccoli L, Müller U, Fontana P (2014) Mechanical behavior of earthen materials: a comparison between earth block masonry, rammed earth and cob. Constr Build Mater 61:327–339

[11] Abrams DP (2001) Performance based engineering concepts for unreinforced masonry building structures. Prog Struct Eng Mat 3:48–56

[12] Bui QB, Morel JC (2009) Assessing the anisotropy of rammed earth. Constr Build Mater 23:3005–3011

[13] Damjamic F, Owen D (1984) Practical considerations for modeling of post-cracking concrete behavior for finite element analysis of reinforced concrete structures. In: Proceedings of the international conference on computer aided analysis and design of concrete structures, 693–706

LIST OF TABLE CAPTIONS

Table 1 Results from cyclic tests at different limit states

Table 1 Results from cyclic tests at different limit states

Sample	H_f (kN)	δ_f (mm)	θ_f (%)	δ_{cr} (kN)	θ_{cr} (mm)	θ_{cr} (%)	H_{max} (kN)	δ_{max} (mm)	θ_{max} (%)	H_u (kN)	δ_u (mm)	θ_u (%)	Failure mode
REW1	39.2	1.6	0.12	58.7	3.6	0.12	73.8	6.8	0.52	73.8	6.8	0.52	Shear
REW2	35.2	1.8	0.14	49.9	3.9	0.14	59.7	6.1	0.47	59.1	6.9	0.53	Shear
REW3	40.3	1.7	0.13	65.0	4.7	0.13	77.6	7.1	0.55	76.6	9.0	0.69	Shear

Table 2 Mechanical properties for numerical analysis

Table 2 Mechanical properties for numerical analysis

TSCRM						
Material	E (N/mm^2)	ν (-)	f_c (N/mm^2)	G_c (N/mm)	f_t (N/mm^2)	G_f^I (N/mm)
Rammed Earth	4207	0.27	3.7	5.98	0.37	0.11
Coulomb friction model						
Material	k_n (N/mm^3)	k_s (N/mm^3)	c (N/mm^2)	tan(φ) (-)	tan(ψ) (-)	f_t^i (N/mm^2)
Interfaces	42.1	16.6	0.56	0.75	0	0.25

Table 3 Values of the numerically derived shear force in kN at peak displacement in each loading sequence for different material properties (% difference from initial analysis in brackets)

Table 3 Values of the numerically derived shear force in kN at peak displacement in each loading sequence for different material properties (% difference from initial analysis in brackets)

Parameters considered		G_f^I (N/mm)				f_t (N/mm²)				c (N/mm²)				*v* (-)			
		0.022 [a]		0.545 [b]		0.19 [a]		0.74 [b]		0.281 [a]		1.122 [b]		0.10 [a]		0.40 [b]	
δ (mm)	H (kN)	H (kN)				H (kN)				H (kN)				H (kN)			
Actuator extension																	
2.5	80	79	(-1.3%)	79	(-1.3%)	75	(-6.3%)	80	(0.0%)	80	(0.0%)	80	(0.0%)	80	(0.0%)	79	(-1.3%)
5.0	95	96	(1.1%)	94	(-1.1%)	67	(-29.5%)	95	(0.0%)	94	(-1.1%)	94	(-1.1%)	94	(-1.1%)	94	(-1.1%)
7.5	79	89	(1.3%)	71	(-11.3%)	65	(-18.8%)	91	(13.8%)	65	(-18.8%)	79	(-1.3%)	78	(-2.5%)	83	(3.8%)
10.0	63	20	(-68.8%)	73	(14.1%)	65	(1.6%)	77	(20.3%)	66	(3.1%)	62	(-3.1%)	63	(-1.6%)	59	(-7.8%)
12.5	64	0	(-100.0%)	76	(18.8%)	65	(1.6%)	73	(14.1%)	67	(4.7%)	65	(1.6%)	64	(0.0%)	62	(-3.1%)
Actuator retraction																	
2.5	80	79	(-1.3%)	80	(0.0%)	16	(-80.0%)	80	(0.0%)	81	(1.3%)	81	(1.3%)	81	(1.3%)	80	(0.0%)
5.0	90	91	(1.1%)	89	(-1.1%)	32	(-64.4%)	95	(5.6%)	88	(-2.2%)	95	(5.6%)	95	(5.6%)	95	(5.6%)
7.5	63	25	(-60.9%)	76	(18.8%)	44	(-31.3%)	90	(40.6%)	63	(-1.6%)	73	(14.1%)	69	(7.8%)	49	(-23.4%)
10.0	57	12	(-78.9%)	76	(33.3%)	50	(-12.3%)	77	(35.1%)	63	(10.5%)	61	(7.0%)	67	(17.5%)	37	(-35.1%)
12.5	50	0	(-100.0%)	76	(55.1%)	50	(2.0%)	75	(53.1%)	56	(14.3%)	61	(24.5%)	67	(36.7%)	36	(-26.5%)
Parameters considered		tan(φ) (°)				f_t^i (N/mm)				f_c (N/mm²)				E (N/mm²)			
		20 [a]		50 [b]		0.125 [a]		0.500 [b]		2.93 [a]		4.40 [b]		2140 [a]		8414 [b]	
δ (mm)	H (kN)	H (kN)				H (kN)				H (kN)				H (kN)			
Actuator extension																	
2.5	80	80	(0.0%)	79	(-1.3%)	80	(0.0%)	81	(1.3%)	77	(-3.8%)	81	(1.3%)	76	(-5.0%)	80	(0.0%)
5.0	95	95	(0.0%)	95	(0.0%)	94	(-1.1%)	91	(-4.2%)	91	(-4.2%)	96	(1.1%)	92	(-3.2%)	94	(-1.1%)
7.5	79	82	(2.5%)	69	(-13.8%)	79	(-1.3%)	61	(-23.8%)	72	(-10.0%)	83	(3.8%)	78	(-2.5%)	81	(1.3%)
10.0	63	55	(-14.1%)	71	(10.9%)	62	(-3.1%)	60	(-6.3%)	57	(-10.9%)	66	(3.1%)	72	(12.5%)	70	(9.4%)
12.5	64	53	(-17.2%)	70	(9.4%)	60	(-6.3%)	59	(-7.8%)	59	(-7.8%)	65	(1.6%)	41	(-35.9%)	0	(-100.0%)
Actuator retraction																	
2.5	80	81	(1.3%)	81	(1.3%)	80	(0.0%)	81	(1.3%)	78	(-2.5%)	82	(2.5%)	77	(-3.8%)	80	(0.0%)
5.0	90	90	(0.0%)	80	(-11.1%)	92	(2.2%)	91	(1.1%)	90	(0.0%)	93	(3.3%)	90	(0.0%)	87	(-3.3%)
7.5	63	66	(3.1%)	57	(-10.9%)	70	(9.4%)	57	(-10.9%)	72	(12.5%)	67	(4.7%)	77	(20.3%)	80	(25.0%)
10.0	57	64	(12.3%)	57	(0.0%)	67	(17.5%)	47	(-17.5%)	57	(0.0%)	67	(17.5%)	73	(28.1%)	74	(29.8%)
12.5	50	65	(32.7%)	61	(24.5%)	66	(34.7%)	46	(-6.1%)	59	(20.4%)	64	(30.6%)	52	(6.1%)	0	(-100.0%)

a = lower value, b = upper value

Table 4 Recommended values for the numerical analysis of rammed earth with the TSRCM and the Coulomb friction model (a = from testing)

Table 4 Recommended values for the numerical analysis of rammed earth with the TSRCM and the Coulomb friction model (a = from testing)

TSRCM

Material	E (N/mm^2)	ν (-)	f_c (N/mm^2)	G_c (N/mm)	f_t (N/mm^2)	G_f^I (N/mm)
Rammed earth	[a]	[a]	Multi-linear relationship [a]	Multi-linear relationship [a]	(0.08-0.12) f_c	(0.10-0.50) f_t *(N/mm^2)*
Coulomb friction model						
Material	k_n (N/mm^3)	k_s (N/mm^3)	c (N/mm^2)	$\tan(\phi)$ (-)	$\tan(\psi)$ (-)	f_t^i (N/mm)
Interfaces	E/100 (N/mm^2)	$k_s = \frac{k_n}{2(1+\nu)}$	(1.5-2.0) f_t	0.58-1.00	0	(0.67-1.00) f_t

LIST OF FIGURE CAPTIONS

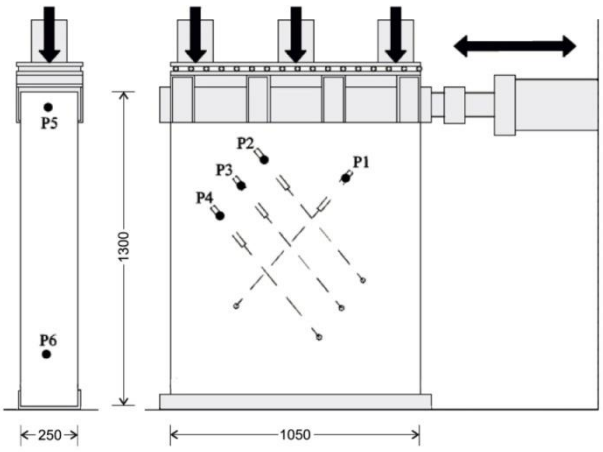

Fig. 1. Scheme of the cyclic in-plane shear-compression test and the placement of sensors (P1–P6)

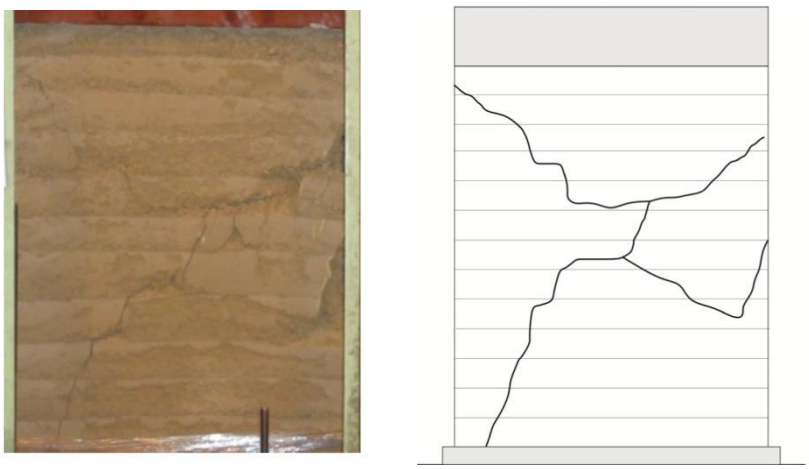

Fig. 2. Crack pattern of one of the rammed earth walls under a combination of vertical compression and cyclic shear (REW1)

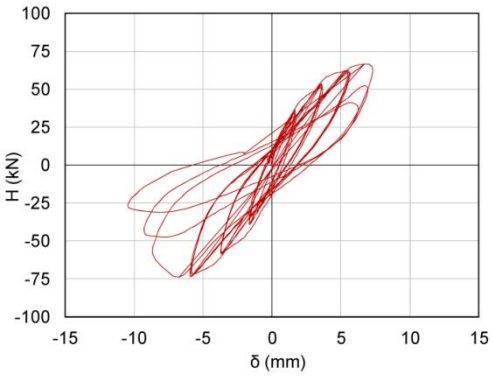

Fig. 3. Experimental hysteresis loops of one of the rammed earth walls (REW1)

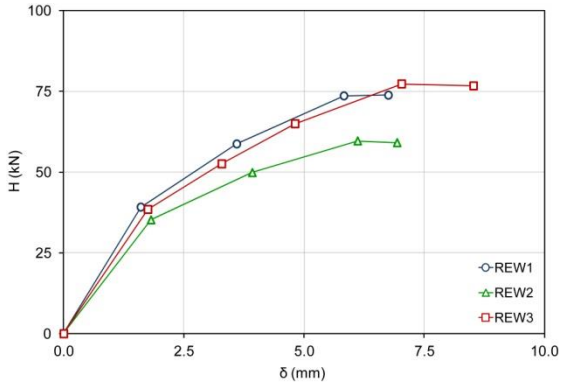

Fig. 4. Shear-compression envelope curves of rammed earth walls

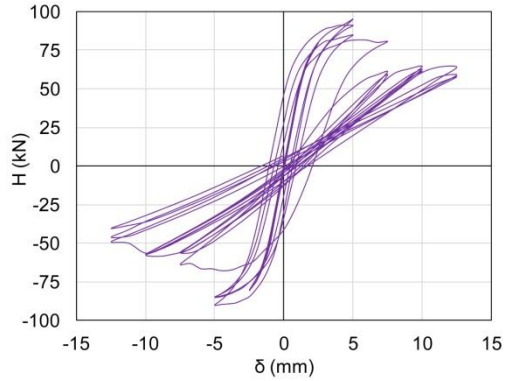

Fig. 5. Numerically derived hysteresis loops from the numerical analysis

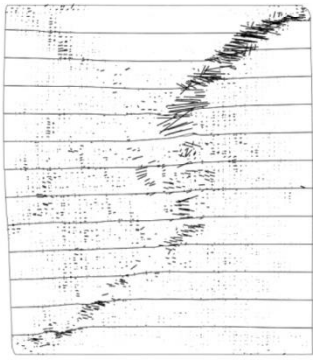

$\tau = 0.24$ N/mm^2

Fig. 6. Crack pattern under cyclic loading at the last level of displacement (12.5 mm)

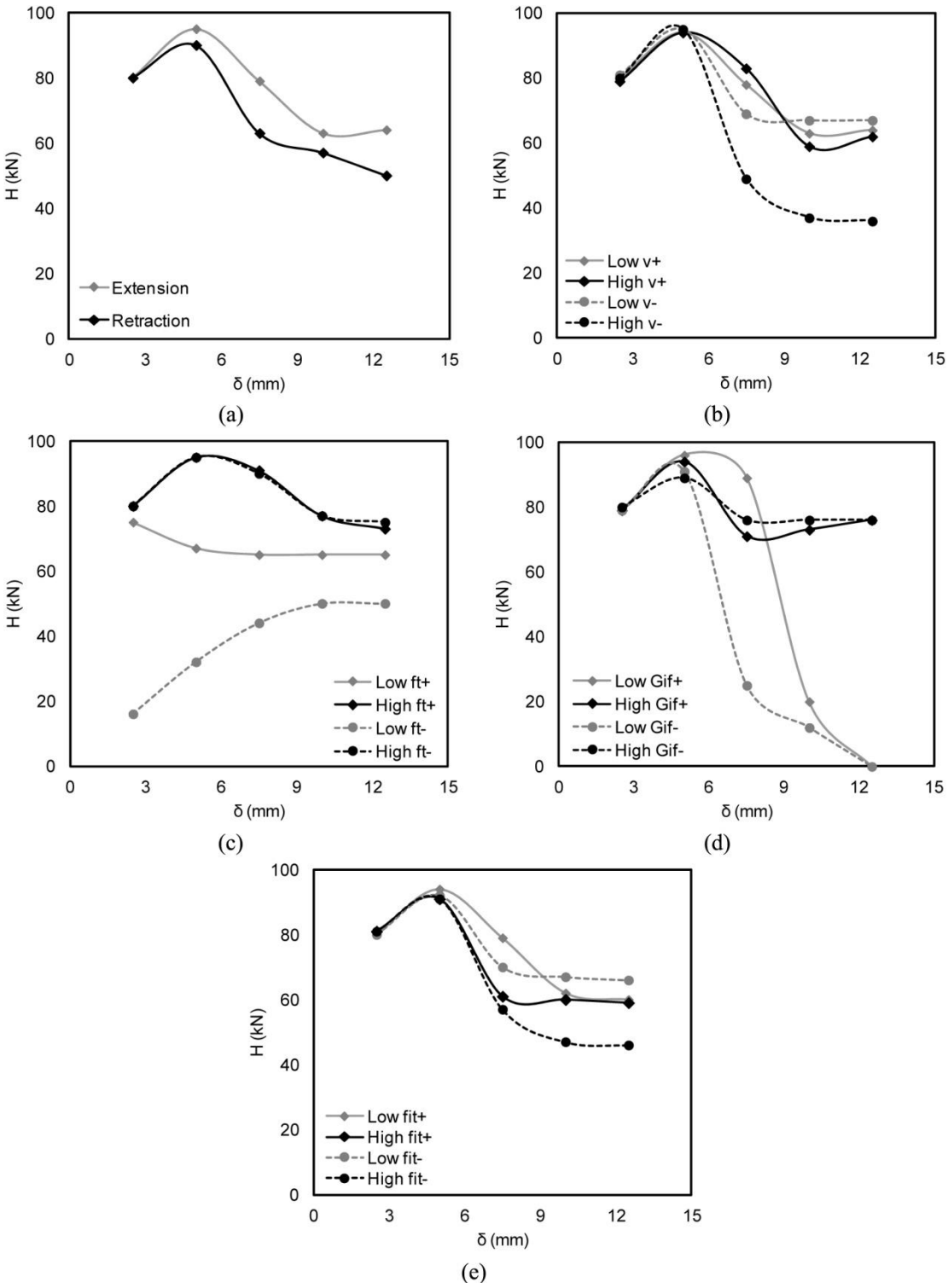

Fig. 7. Effect of the horizontal load on the displacement for different levels of the parameter assessed for actuator extension (+) or retraction (-)(a), ν (b), f_t (c), G^I_f (d), and f^i_t (e)